Available online at www.eccomasproceedia.org
Eccomas Proceedia COMPDYN (2023) 5089-5101

ECCOMAS
Proceedia

COMPDYN 2023
9th ECCOMAS Thematic Conference on
Computational Methods in Structural Dynamics and Earthquake Engineering
M. Papadrakakis, M. Fragiadakis (eds.)
Athens, Greece, 12-14 June 2023

INELASTIC TORSIONAL BUCKLING OF A SYMMETRIC THREE-DIMENSIONAL MOMENT-RESISTING FRAME SUBJECTED TO HORIZONTAL FORCE IN THE DIAGONAL DIRECTION

Iori Fukuda[1], Kohju Ikago[1],
Takahito Maeda[2], Atsushi Nishimoto[3], and Yoshikazu Araki[2]

[1] Tohoku University
468-1-E402(IRIDeS), Aoba Aramaki, Aoba-ku, Sendai, 980-8572, Japan
iori.fukuda.q3@dc.tohoku.ac.jp, ikago@irides.tohoku.ac.jp

[2] Nagoya University
ES538, Chikusa, Nagoya, 464-8603, Japan
yoshikazu.araki@nagoya-u.jp, maeda.takahito.1019@gmail.com

[3] NIKKEN SEKKEI LTD
4-15-32, Sakae, Naka-ku, Nagoya, 460-0008, Japan
nishimoto.atsushi@nikken.jp

Abstract

In this study, numerical analyses demonstrate that a simple symmetrical 3D steel moment resisting frame with slight eccentricity can exhibit torsional behaviour despite a diagonal load being applied in a perfectly symmetrical manner. The torsion may be caused by inelastic bifurcation buckling, where the combined effect of the material and geometrical nonlinearity plays an important role. The similarities between this phenomenon and the inelastic buckling theories found in the literature are discussed.

Keywords: Inelastic Buckling, Geometrical Nonlinearity, Torsion, Moment Resisting Frame, 3D, Numerical Analysis

ISSN:2623-3347
Peer-review under responsibility of the organizing committee of COMPDYN 2023.
doi: 10.7712/120123.10785.21142

1 INTRODUCTION

Although sophisticated analytical software allows the analysis of complicated large-scale structural models, epistemic uncertainties remain in the numerical analysis technique for tracing the inelastic torsional behaviour of three-dimensional (3D) frames. Researchers have reported that various uncertainties and irregularities in the stiffness and mass distribution leading to eccentricity as well as combined nonlinearity cause torsion. For example, Kohiyama and Yokohama [1] highlighted the existence of a geometrical nonlinearity referred to as the Q-Delta effect and evaluated its influence on the elastic torsional response. Flores *et al*. [2] conducted numerical analyses of frames considering the material and geometrical nonlinearities and demonstrated the importance of geometrical nonlinearities, namely, the P-Theta effect [3] and the P-Delta effect. Additionally, studies regarding the torsional behaviour of a perfectly symmetrical frame with no irregularities subjected to a symmetrical load are limited, while accidental torsion has been well-studied and considered in the structural design in practice.

In this study, quasi-static and dynamic analyses demonstrate that a simple symmetrical 3D steel moment resisting frame (SMRF) with slight eccentricity can undergo drastic torsional behaviour, despite a diagonal load being applied in a symmetric and deterministic manner. Namely, torsional behaviour in a structure can occur without irregularities in loading as well as in mass and stiffness distributions. Moreover, analysis demonstrates that the torsion is caused by inelastic bifurcation buckling, which is proven by the similarity between the results of the quasi-static analysis and inelastic column theory by Shanley [4], as well as the agreement between the results and the predicted behaviour presented in studies by Fukuda and Ikago [5, 6], who theoretically considered the torsion of an SMRF owing to inelastic bifurcation buckling. OpenSees [7] is used as the analysis framework, in which the combined effect of the material and geometrical nonlinearity is considered.

2 MODEL AND ANALYSIS CONDITIONS

2.1 Overview of the model

Consider a one-bay, one-storey, and perfectly symmetric SMRF, as shown in Figure 1, where pins support the bottom of the columns. The span and storey height are both 4 m. Here, (1), (2), (3), and (4) shown in Figure 1 indicate the number of the frames; the red arrows indicate the global axis of the coordinates. Regarding the beams in this model, only the in-plane bending stiffness is considered, while the torsional and out-of-plane bending stiffness are neglected. Euler-Bernoulli beam-column elements are used; the beams are connected to the nodes via bi-linear rotational spring elements. The yielding stress of the beams in frames (1) and (2) is reduced by 1% relative to that of frames (3) and (4), introducing an initial imperfection. The tops of the columns are connected to a rigid floor diaphragm, and its central node is referred to as the ‘master node’ hereafter. The in-plane rotation angle of the rigid diaphragm around the vertical axis is represented by θ, as shown in Figure 1. The master node and the ground are connected by elastic horizontal shear springs to ensure the stability of the model after yielding of the beam-end rotational spring elements. Note, these shear springs are not arranged in the global X and Y directions, but in the direction parallel to frames (1) and (4). Finally, the lumped mass and mass moment of inertia are placed at the master node.

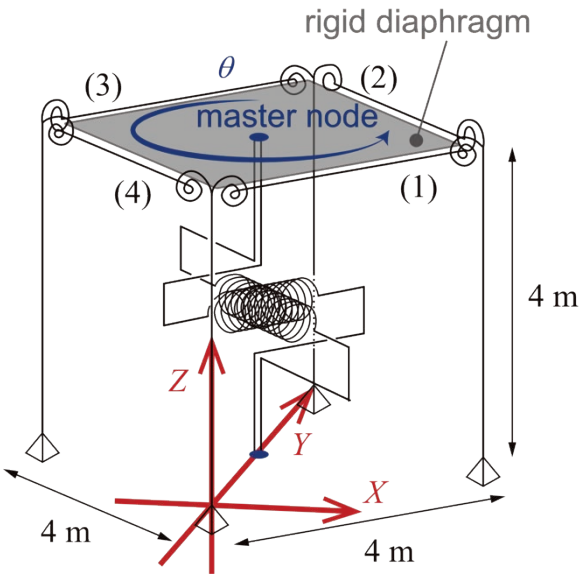

Figure 1: SMRF model

2.2 Member specifications, constitutive law of materials, and mass (moment of inertia)

The columns and beams are steel members (Young's modulus $E = 2.05 \times 10^8$ kN/m^2), which have box- (Figure 2(a)) or wide-flange shaped (Figure 2(b)) cross sections, respectively. The dimensions and specifications of the columns and beams are given in Table 1. Here, the local axes of the members are shown in Figure 2(a, b); the local z-axis direction of the beam shown in Figure 2(b) coincides with the global Z-axis direction shown in Figure 1. An infinitesimal value (10^{-15}) was assigned for the neglected stiffness, which can be regarded as zero in the numerical analysis.

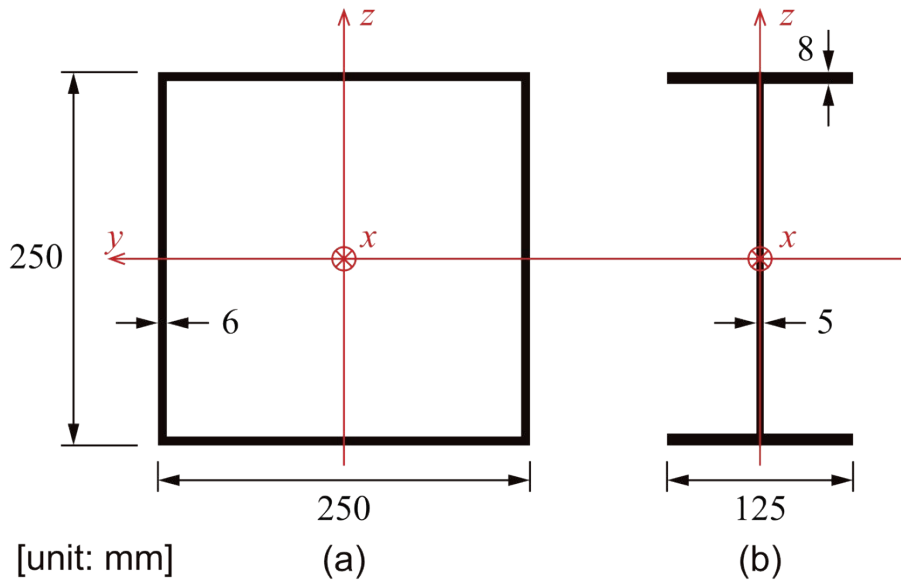

Figure 2: Cross section of the (a) columns and (b) beams

Considering the bilinear hysteresis of the beams, the initial stiffness $k_{Ry} = 6EI_y/l$ corresponds to the bending stiffness of the Euler-Bernoulli element subjected to an asymmetrical bending moment (Figure 3). The ratio of the initial and post-yielding stiffnesses is $\alpha = 0.01$. The yielding bending moment of the beams of frames (3) and (4) is $M_{\text{yield}} = 32$ kN, and that of

frames (1) and (2) is 31.68 kN (= $M_{yield} \times 0.99$). The stiffness of the elastic horizontal shear springs between the master node and the ground is 40 kN/m in both directions.

	Columns	Beams
Dimension	250 × 250 × 6 mm	250 × 125 × 5 × 8 mm
Length: l	4 m	
Cross sectional area: A	5.763×10^{-3} m^2	3.199×10^{-3} m^2
Second moment of area about the local y-axis: I_y	5.67×10^{-5} m^4	3.45×10^{-5} m^4
Second moment of area about the local z-axis: I_z		10^{-15} m$^4 \approx 0$ (ignored)
St. Venant torsional constant of the cross section: J_x	10^{-15} kNm/rad ≈ 0 (bottoms are pin-supported)	10^{-15} kNm/rad ≈ 0 (ignored)

Table 1: Specifications of members

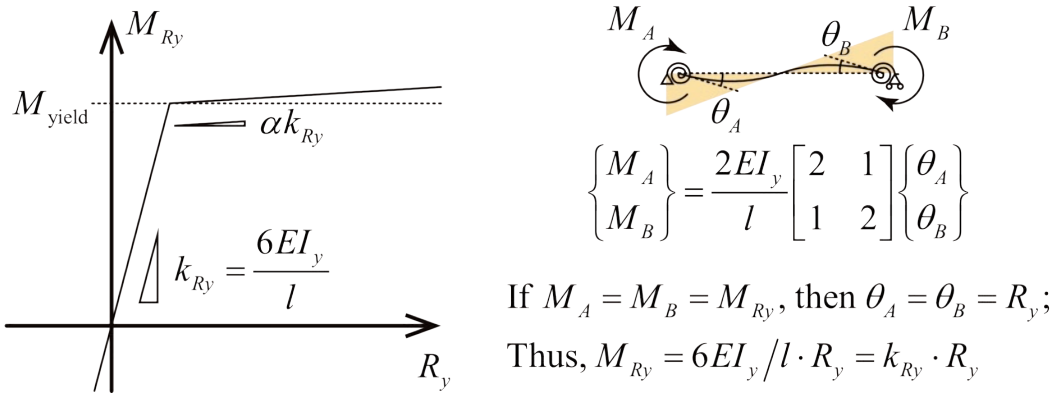

Figure 3: Nonlinear constitutive law of beam-ends

The mass in the global X and Y directions, represented by m_X and m_Y, respectively, are placed at the master node, while that for the global Z direction, m_Z, is neglected. Furthermore, only the mass moment of inertia around the Z-axis, ${}_Z I_m$, is considered and placed at the master node, while the mass moment of inertia around the X- and Y-axis, represented by ${}_X I_m$ and ${}_Y I_m$, respectively, are neglected. Note, an infinitesimal value (10^{-15}) was assigned for the neglected mass or mass moment of inertia. The mass is calculated provided that the mass per unit area at the top floor is 0.8 ton/m^2, and its distribution is uniform (0.8 ton/m^2 × 4 m × 4 m = 12.8 ton). ${}_Z I_m$ is calculated using Equation (1), assuming that the lumped masses of 1/4 of the total mass, that is, 3.2 ton, were located at the centre of each quarter block shown in Figure 4(a).

$$ {}_Z I_m = \sum_i^n r_i^2 \cdot m_i \tag{1} $$

Here, n is the total number of lumped masses ($n = 4$), r_i ($i = 1, 2, \ldots, n$) is the distance from the master node to each lumped mass (uniformly $r_i = \sqrt{2}$ m), and m_i ($i = 1, 2, \ldots, n$) represents the lumped mass ($m_i = 3.2$ ton for each i); therefore, ${}_Z I_m$ is 25.6 ton·m^2. In this study, two comparison models were also employed, whose r_i values were 1 and $1/\sqrt{2}$ m, respectively (Figure 4(b)). Their ${}_Z I_m$ values were also calculated by the same procedure; ${}_Z I_m = 12.8$ ton·m^2 and ${}_Z I_m = 6.4$ ton·m^2 for $r_i = 1$ and $r_i = 1/\sqrt{2}$, respectively.

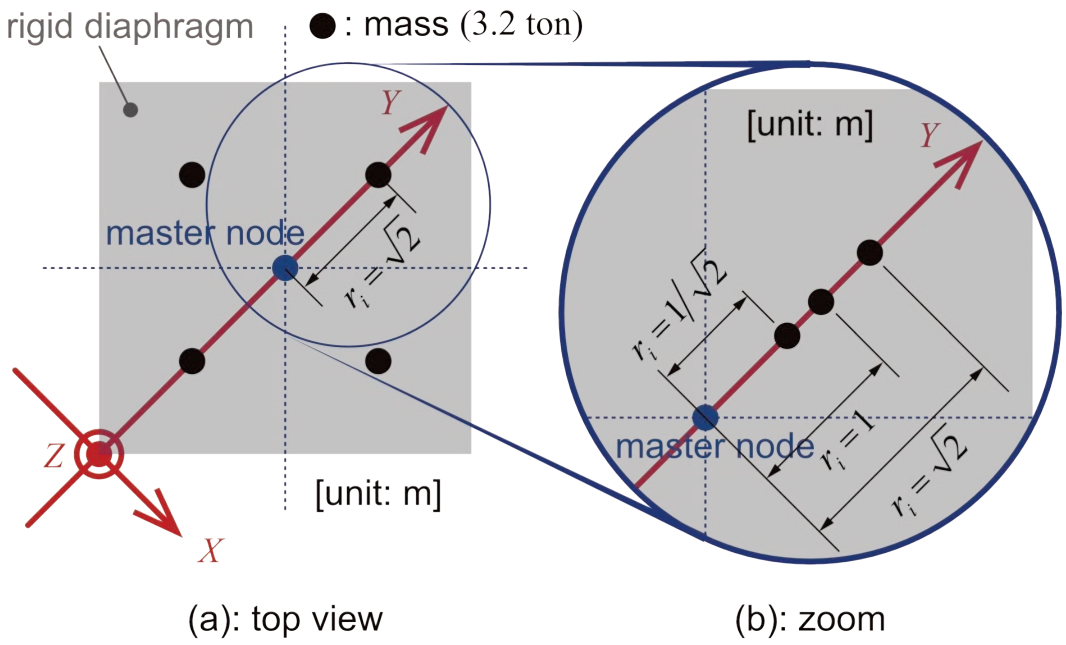

Figure 4: Calculation of the moment of inertia

Table 2 presents the 1st to 3rd natural periods of these models. The 1st and 2nd natural periods of all the models are identical. Figure 5(a–c) depicts the 1st to 3rd eigenmodes of the model whose $r_i = \sqrt{2}$. The 1st eigenmode exhibits a drift in the loading direction, as shown in Fig. 5(a), the 2nd eigenmode exhibits a drift in the orthogonal direction of loading, as shown in Fig. 5(b), and the 3rd eigenmode is a torsional mode, as shown in Fig. 5(c).

	$r_i = \sqrt{2}$ m	$r_i = 1$ m	$r_i = 1/\sqrt{2}$ m
1st natural period	0.690 s		
2nd natural period	0.509 s		
3rd natural period	0.307 s	0.217 s	0.153 s

Table 2: 1st to 3rd natural periods of the models

2.3 Analysis cases

For all the analysis cases, a vertical load of 31.36 kN that was divided into 10 000 steps was incrementally applied on the top of the columns. This vertical load was also calculated based on the assumption that the mass per unit area, 0.8 ton/m^2, was uniformly distributed.

Two types of horizontal loading analyses were performed, namely quasi-static and dynamic. In both cases, the degree of freedom in the X-axis was not fixed. In the quasi-static analysis, a load of 55 kN that was divided into 100 000 steps was incrementally applied to the master node from the global Y-axis direction. In the dynamic analysis, a 1940 El Centro NS wave whose peak ground velocity (PGV) was scaled to 100 cm/s was input in the global Y-axis direction for each model. The duration of the analysis was set to 80 s to examine the free vibration after the seismic input ended. A time interval of 0.001 s was used for the numerical integration. We assume an initial stiffness-proportional damping, where the damping ratio for the 1st mode h_1 was 2% to the critical damping coefficient.

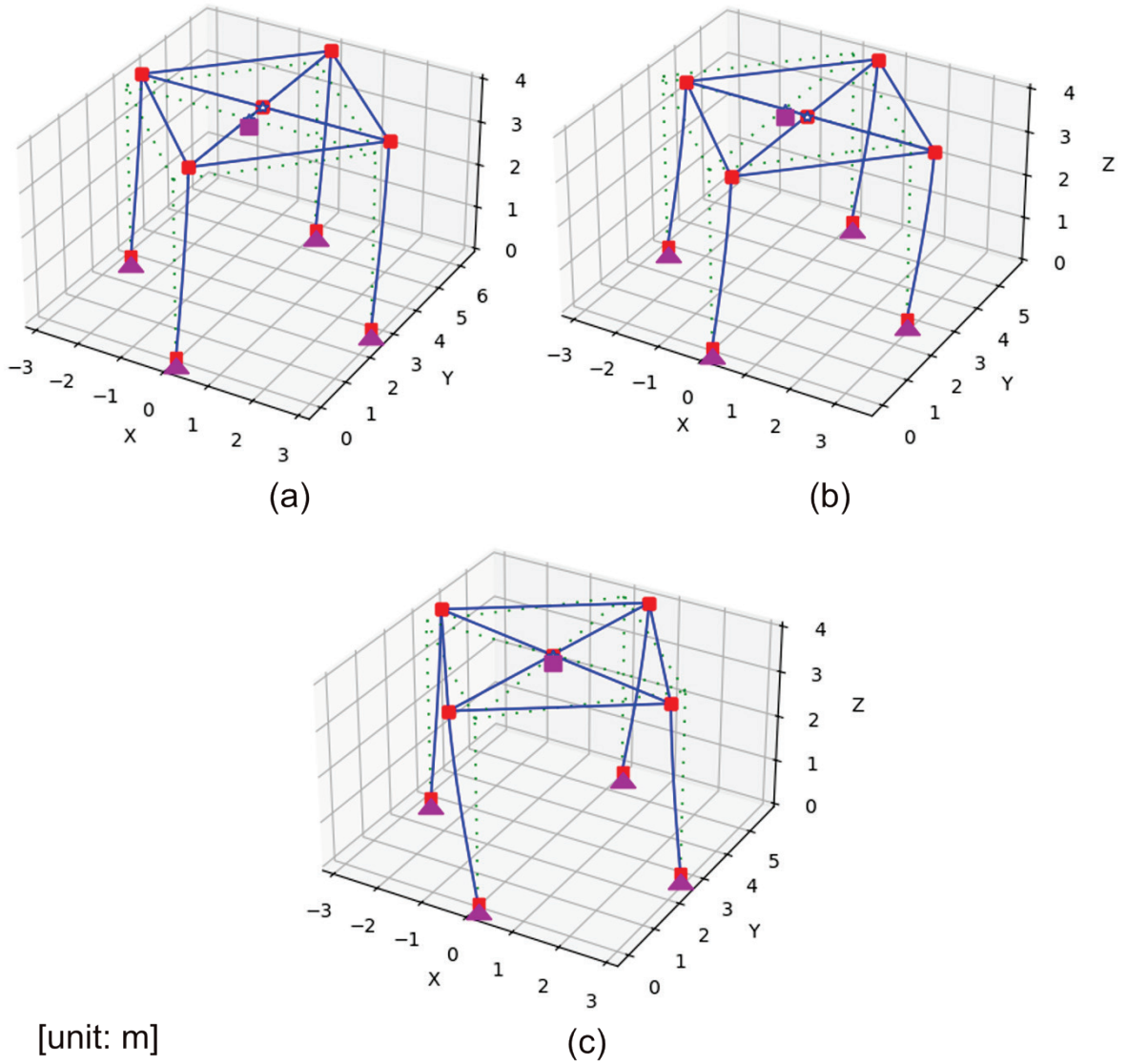

Figure 5: The (a) 1st, (b) 2nd, and (c) 3rd mode shapes of the $r_i = \sqrt{2}$ model

2.4 Modeling in OpenSees

The elasticBeamColumn elements were used for the Euler-Bernoulli elements. The bilinear rotational springs at the beam ends are implemented by zeroLength elements. Double nodes are created at each beam-end to insert the zeroLength elements. The elastic horizontal shear springs are represented by an equivalent zeroLength element, and a double node at the location of the master node is created to insert the zeroLength element. Steel01 and Elastic uniaxialMaterial are used to represent the hysteresis of the elastoplastic hinges and the elastic horizontal shear springs, respectively. The rigid floor diaphragm is implemented using elasticBeamColumn elements, where sufficiently large or small values (10^{10} and 10^{-15}, respectively) that numerically represent the rigid or pin connection are assigned to the cross-sectional area and bending stiffness. The PDelta option of the geomTransf command is specified to account for the geometrical nonlinearity of the columns. The PDelta option assumes finite deformations, that is, the rotational deformation of the columns, φ, is small, and the approximations of $\sin\varphi \approx \varphi$ and $\cos\varphi \approx 1$ are valid. The geometrical stiffness matrix is calcu-

lated with this 1st order approximation and subtracted from the tangent stiffness matrix [8]. The other options are summarised in Table 3.

	Gravity Loading	Horizontal Loading	
		Quasi-static	Dynamic
constraints	Penalty 1.0e+15 1.0e+15	Pentalty 1.0e+18 1.0e+18	
numberer	RCM	RCM	
system	SparseGEN (SuperLU)	FullGeneral	
test	NormDispIncr 1.0e-8 100	NormDispIncr 1.0e-2 1000	
algorithm	NewtonLineSearch -maxIter 10000	Broyden -count 50	
integrator	LoadControl	LoadControl	Newmark 0.5 0.25
analysis	Static	Static	Transient

Table 3: Options of OpenSees

3 RESULTS OF NUMERICAL ANALYSIS

This section first presents the quasi-static analysis results and demonstrates that torsion can occur even in a symmetrical SMRF with an infinitesimal stiffness eccentricity, whose effect is generally considered to be negligible. Second, the fact that the torsion was apparently caused by inelastic bifurcation buckling is presented, followed by the discussion regarding the similarity between the analytical results and the inelastic column buckling theory proposed by Shanley [4]. Finally, the dynamic analysis results reveal that torsional deformation occurred in the seismic response of these models, and the extent of torsion was influenced by the mass moment of inertia associated with the torsional resistance of the model.

3.1 Quasi-Static Analysis

Figure 6 depicts the step histories of the master node in the X-, Y-, and θ-directions, demonstrating that the torsional deformation θ occurs near step 82 000; thereafter, displacements in the θ- and Y-directions significantly increase. Namely, a torsion can occur even in a symmetrical SMRF with an infinitesimal stiffness eccentricity. Note, displacement also occurs in the orthogonal X-direction to loading, but its overall effect is small because the increasing rate of the X-displacement is smaller than that in the Y- and θ-directions. Figure 7 depicts the overall deformation at the end of loading without any scale factor, confirming that the contribution of the X-displacement to the overall deformation is insignificant.

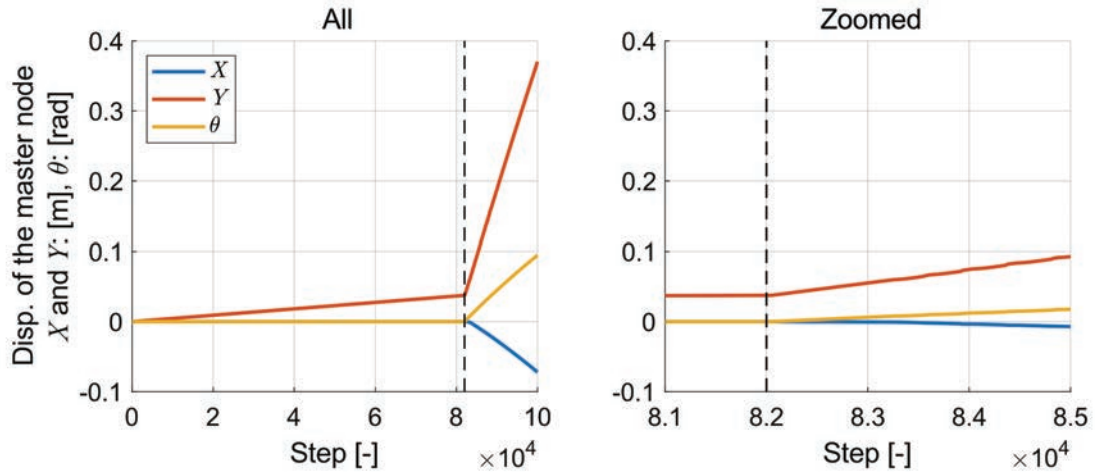

Figure 6: Step history of the master node displacement

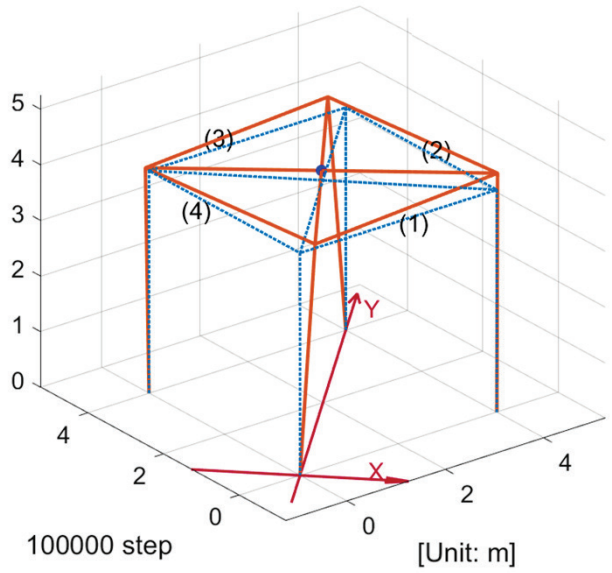

Figure 7: Global deformation of the SMRF model at 100 000 steps

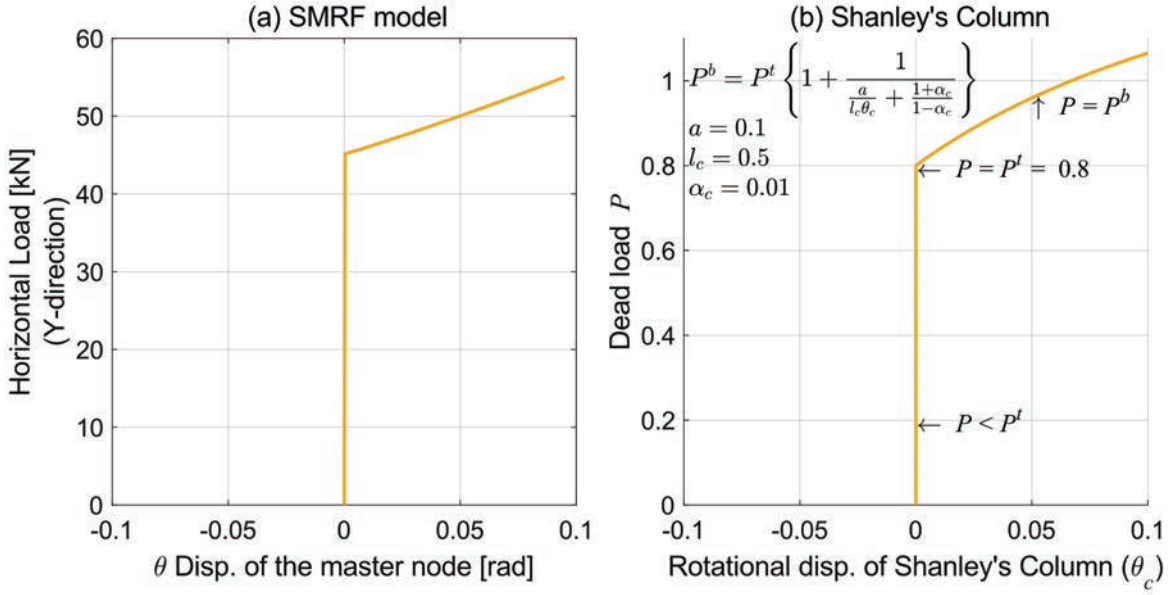

Figure 8: (a) Relationship of the horizontal load–master node θ of the SMRF model, and (b) P–θ_c relationship of the Shanley Column

The horizontal load–θ relationship in this SMRF model, Figure 8(a), is one source of evidence that suggests that this torsion is inelastic bifurcation buckling. This is because a similar relationship (Figure 8(b)) can be found in an inelastic buckling problem of a centre-compressed short column discussed by Shanley [4] (Figure 9, designated Shanley's Column here). If a bifurcation occurs at the tangent modulus load P^t in a Shanley's Column with elastoplastic springs whose hysteresis is bilinear, the load after the bifurcation P^b and the buckling deformation θ_c satisfy the following relationship.

$$P^b = P^t \left\{ 1 + \frac{1}{a/l_c\theta_c + (1+\alpha_c)/(1-\alpha_c)} \right\} \tag{2}$$

where a and l_c are the parameters related to the dimensions of the Shanley's Column, and α_c is the tangent stiffness ratio of the elastoplastic springs. Figure 8(b) is based on the following conditions: $P^t = 0.8$, $a = 0.1$, $l_c = 0.5$, and $\alpha_c = 0.01$. Based on this similarity, a load-controlled inelastic torsional bifurcation theory should be developed for the SMRF used in this study, and a relationship of the horizontal load–master node θ similar to Equation (2) can also be derived.

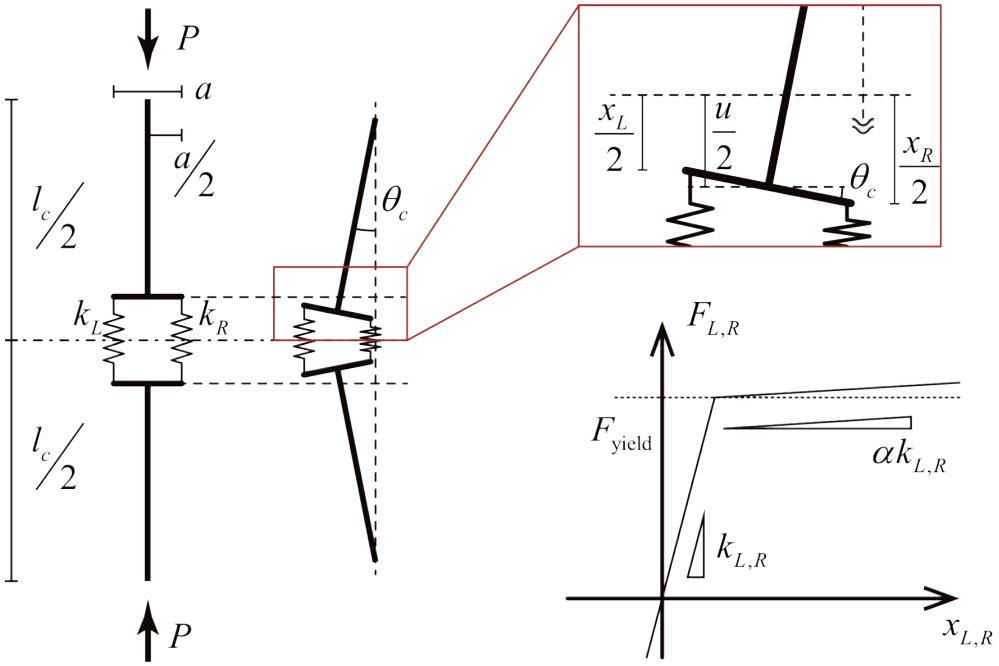

Figure 9: Shanley's Column model

Another source of evidence that suggests that this torsion is an inelastic bifurcation is shown in Figure 10, which depicts the displacements of the rigid diaphragm and the yielding status of the beam-ends at every 1000 steps from steps 82 000 to 85 000. This verifies the results discussed in the study by Fukuda and Ikago [5, 6], who theoretically investigated the inelastic torsional bifurcation of a simple SMRF under limited conditions. According to Fukuda and Ikago [5, 6], if the SMRF used in this study is subjected to a controlled load or controlled displacement resulting in torsion, it is expected that the beam-ends of frames (1) and (2) will be in a post-yielding or designated loading state, while that of frames (3) and (4) will be in an elastic or unloading state after the bifurcation. The results shown in Figure 10 are consistent with this prediction, except for step 85 000. Note, this prediction is inspired by the bifurcation process of Shanley's Column revealed in the inelastic column theory as follows [4]: i) When a bifurcation occurs in a Shanley column, one of the two inelastic springs at the centre of the column is in a loading state, and the other spring is in a neutral state, which is neither in a loading nor unloading state, ii) the spring in the neutral state is continuously unloaded immediately after the bifurcation displacement occurs, and iii) subsequently, the states of these springs are fixed in a combination such that one is in a loading state, and the other in an unloading state. A similar process applies to a simple SMRF model in this study as follows: i) When a torsion occurs in this SMRF, a couple of frames orthogonal to one another,

that is, either frames (1) and (2) or frames (3) and (4) are in a state where their beam-ends are in loading, while the other couple are in a state in which their beam-ends are in a neutral state, which is neither in a loading nor unloading state, ii) immediately after the torsion occurs, the beam-ends in the neutral state are unloaded, and iii) subsequently, the state of the couples of frames and their beam-ends are fixed in a combination such that the beam-ends of one couple of frames are in a loading state and those of the other couple of frames are in an unloading state. Because the initial imperfection is intentionally introduced in this study, the frame couple of frames (1) and (2) is the former, and the remaining frames are the latter in this case.

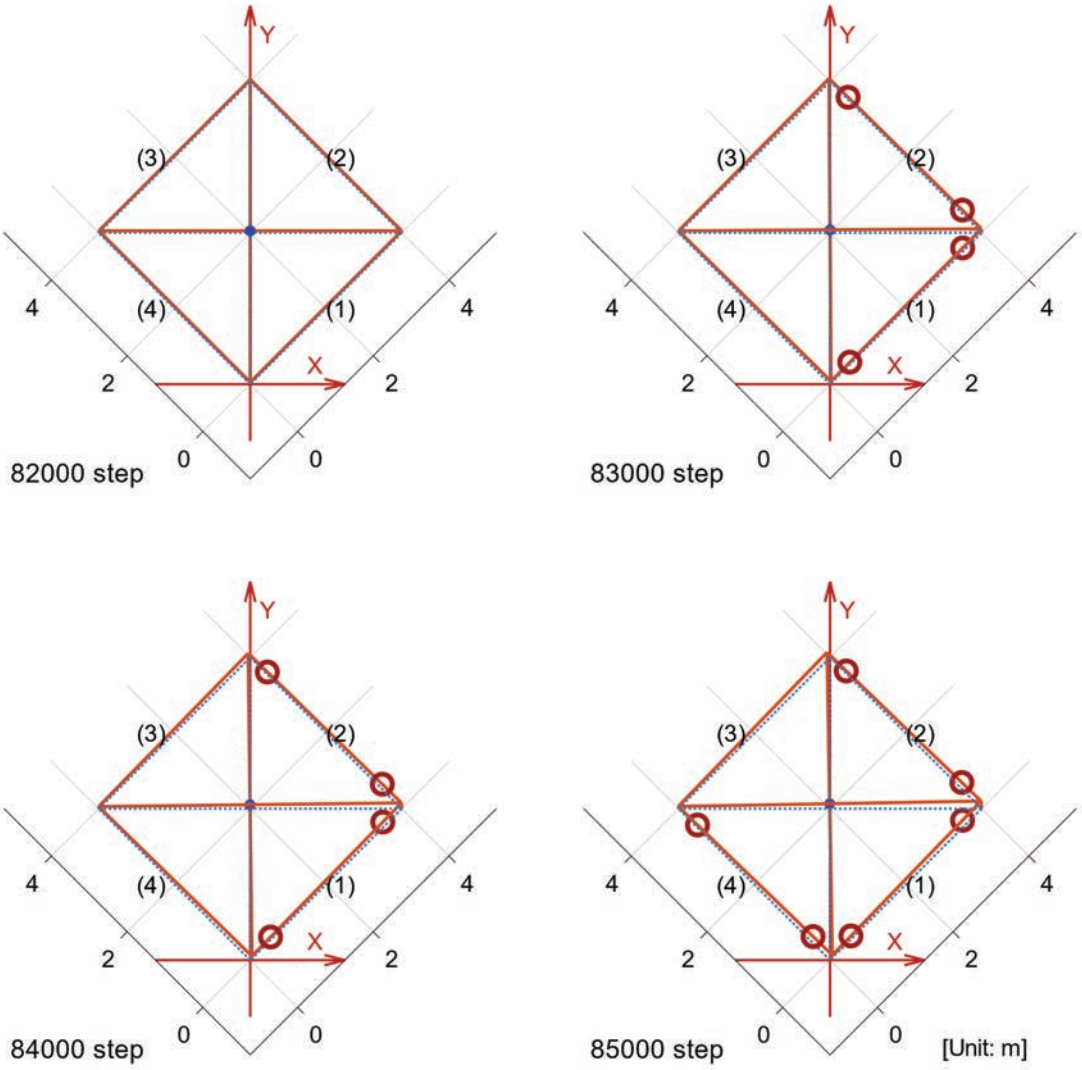

Figure 10: Displacements of the rigid diaphragm and the yielding status of the beam-ends

The yielding state of step 85 000 shown in Figure 10 violates this prediction, which may be related to the *X*-displacement. According to Fukuda and Ikago [6], bifurcation in the orthogonal direction of a controlled displacement can occur in a similar model if the problem considered is displacement-controlled. In these cases, couples of frames change to frames (2) and (4), and frames (1) and (3). A superposition of bifurcation may occur in the torsional and perpendicular directions after step 85 000. As a result, in addition to frames (1) and (2), frame (4)

may also proceed into a yielding state at that time. Note, a load-controlled numerical analysis is conducted in this study, for which the details differ from the theoretical analysis presented by Fukuda and Ikago [6]; therefore, further investigation is required to clarify this behaviour.

3.2 Dynamic Analysis

Figure 11(a–c) presents the time history of the master node displacement for each model and demonstrates that torsion can occur even in a model with infinitesimal eccentricity during the dynamic response. Torsion occurs and increases in the $r_i = 1/\sqrt{2}$ m and $r_i = 1$ m models, whereas almost no torsion can be observed in the $r_i = \sqrt{2}$ m model. Overall, a larger mass moment of inertia results in a smaller torsional deformation.

The main cause of the torsion in this model is unclear at this stage because the damping, instantaneous eccentricity owing to plasticisation, fluctuations in the eigenvalues, Q-Delta effect, as well as inelastic bifurcation buckling, affect the response in a dynamic problem, and the contribution of each factor is complicatedly related to one another. For a clear understanding of this phenomenon, further investigations from various point of views are needed to clarify the contribution of each factor. Therefore, other interesting points relevant to understanding the phenomenon are reserved herein. First, when comparing two models in which torsional deformation occurs (the $r_i = 1/\sqrt{2}$ m and $r_i = 1$ m models), the torsional deformation converges to a constant value in the model with $r_i = 1$ m, whereas the model with $r_i = 1/\sqrt{2}$ m demonstrates a diverging behaviour. However, note that a finite deformation is assumed in this analysis despite the deformation being relatively large. Therefore, the result can be meaningful for tracing the occurrence of a torsion but may underestimate the maximum response compared to the actual behaviour. Second, when comparing the results considering whether torsional deformation occurs, the *X*-axis deformation is apparently related to the torsional deformation. In addition, the $r_i = \sqrt{2}$ m model, which presents a small torsional deformation, demonstrates a free vibration with damping in the *Y*-direction after the seismic excitation ends, whereas the $r_i = 1$ m model, which exhibits converged torsional deformation, exhibits free-vibration behaviour without damping in the *X*- and *Y*-directions.

4 CONCLUSION

In this study, a symmetric SMRF with infinitesimal eccentricity subjected to quasi-static and dynamic horizontal loading in a diagonal direction is examined by a numerical analysis. The results of quasi-static loading indicate that torsion can occur in an SMRF with infinitesimal eccentricity, suggesting that this torsion is caused by inelastic bifurcation buckling. This is demonstrated by the discussion regarding the similarities between the results of the analysis and Shanley's inelastic column theory. One of these similarities is the load–bifurcation displacement relationship, and another similarity is the yielding status of the elastoplastic elements at the beginning of bifurcation. This result partially supports the theoretical predictions by Fukuda and Ikago. In addition, the torsional response in the SMRF also occurs when subjected to dynamic excitation. The degree of torsion depends on the mass moment of inertia that is related to the torsional resistance. Further challenges are identified to determine the contribution of inelastic bifurcation buckling and other factors in the dynamic response.

ACKNOWLEDGEMENTS

This study was supported by the JSPS Grant-in-Aid for the JSPS Research Fellow (Grant Number: JP22J13566).

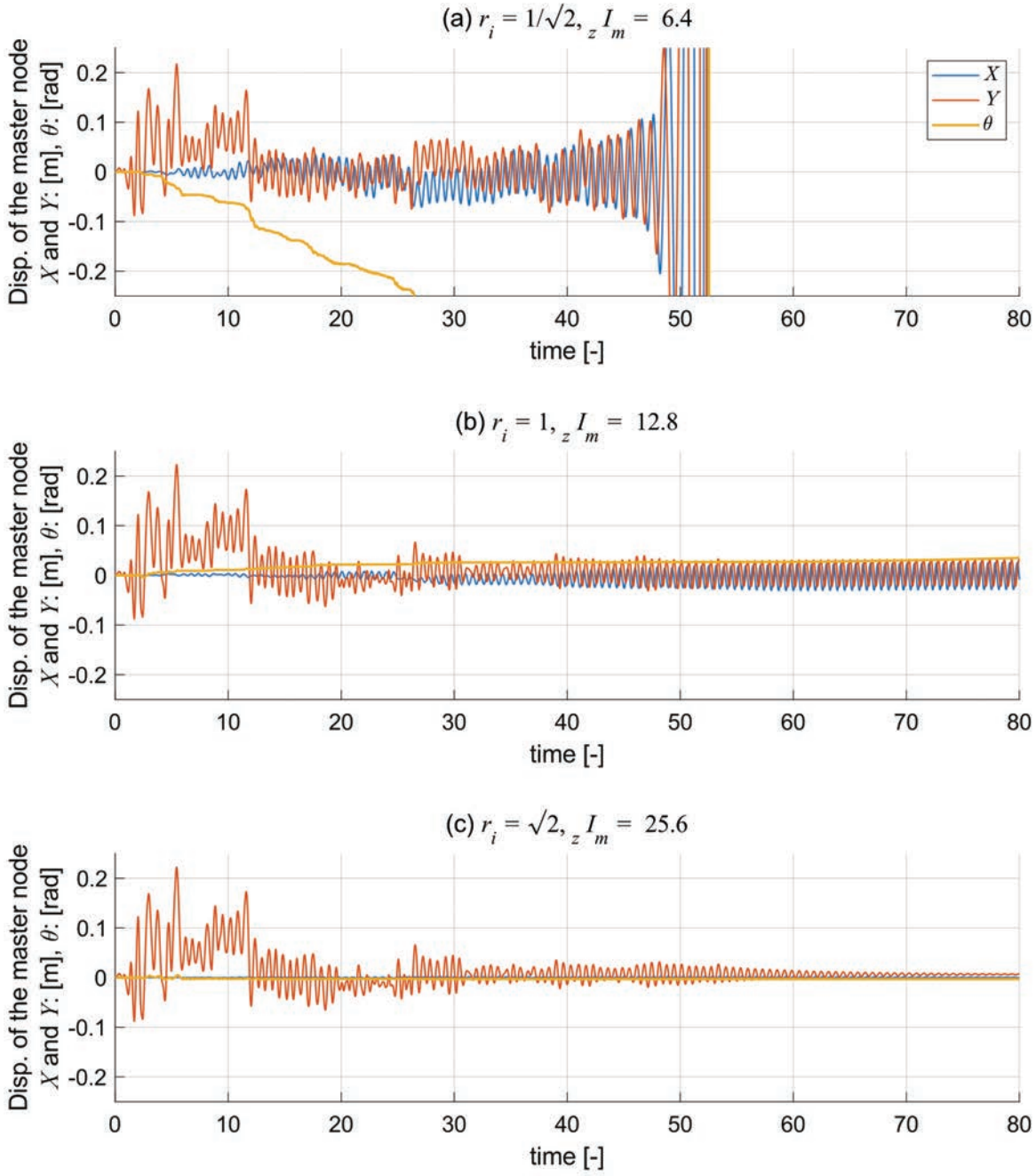

Figure 11: Time history of the master node displacement for each model

REFERENCES

[1] M. Kohiyama, H. Yokoyama, Torsional Response Induced by Lateral Displacement and Inertial Force, *Frontiers in Built Environment*, **4**, 38, 2018.

[2] F. Flores, F.A. Charney, D. Lopez-Garcia, The Influence of Accidental Torsion on the Inelastic Dynamic Response of Buildings during Earthquakes, *Earthquake Spectra*, **34**(1), 21–53, 2018.

[3] E.L. Wilson, A. Habibullah, Static and Dynamic Analysis of Multi-Story Buildings, Including P-Delta Effects, *Earthquake Spectra,* **3**(2), 289–298, 1987.

[4] F.R. Shanley, Inelastic Column Theory, *Journal of the Aeronautical Sciences,* **14**(5), 261–268, 1947.

[5] I. Fukuda, K. Ikago, Global Buckling Analysis of High-Rise Steel Moment-Resisting Frames Involving Inelastic Torsional Deformation Concentration, *12th Pacific Structural Steel Conference*, Tokyo, Japan, November 9–11 2019.

[6] I. Fukuda, K. Ikago, Inelastic Torsional Buckling Analysis of a Single-Story Cubic Frame, *17th World Conference on Earthquake Engineering*, Sendai, Japan, September 27–October 2, 2021. (Postponed from September 13–18, 2020)

[7] https://opensees.berkeley.edu/

[8] M.D. Denavit and J.F. Hajjar, Description of Geometric Nonlinearity for Beam-Column Analysis in OpenSEES, *Department of Civil and Environmental Engineering Reports*, Report No. NEU-CEE-2013-02, Department of Civil and Environmental Engineering, Northeastern University, Boston, Massachusetts, 2013.